HST Kernel-Phase Interferometry: Field Age Brown Dwarf Population Demographics

The University of Texas at Austin
Department of Astronomy
College of Natural Sciences

Samuel M. Factor, Adam L. Kraus
Dept. of Astronomy, The University of Texas at Austin

Contact Information
Email: sfactor@utexas.edu
Website: smfactor.github.io

S. Factor is P.I. of HST cycle 24 & 29 archival projects 14561 & 16612 which support this work.

Kernel-phases are self-calibrating observables **used for high-contrast imaging at or even below λ/D**. We have used this technique to search for companions to brown dwarfs in the *HST* archive and **confirmed a proposed candidate**. We modeled the binary brown dwarf demographics and find a **population favoring tight separation and equal mass companions.** The pipeline will be particularly **applicable to JWST** and future 30m class telescopes and is **available as a python package**.

Background

- While direct-imaging surveys are more sensitive to companions at large semimajor axes than transit and RV surveys, **there is often a gap in sensitivity between direct imaging and transit/RV surveys.**
- "Speckles," caused by imperfections in the optical path (including AO), can be corrected **but most techniques tend to fail near λ/D**.
- Interferometric analysis uses of the wave nature of light to reject speckle noise and detect companions with high contrast *at or even below* the diffraction limit. **Rather than subtracting off the PSF, interferometric techniques use the information contained in it to infer the geometry of the source.**

Filling the gap between transit/RV surveys and classical direct-imaging surveys would offer a crucial new view of both exoplanetary systems and stellar multiplicity. Kernel-phase analysis of *HST/NICMOS* imaging is able to resolve the peak of the separation distribution of field brown dwarfs at significant contrast.

What is a Kernel-Phase?

Non-redundant aperture masking interferometry (NRM or AMI) places a mask in the pupil plane, transforming a large single aperture into a sparse interferometer. This mask blocks ~95% of the gathered light, imposing a *severe* flux limit. **Kernel-phase analysis models the *full aperture* as a grid of sub-apertures** (Fig. 1). This model defines which spatial frequencies are sampled. We then examine the *phase* of the Fourier transform of the images to infer the source geometry.

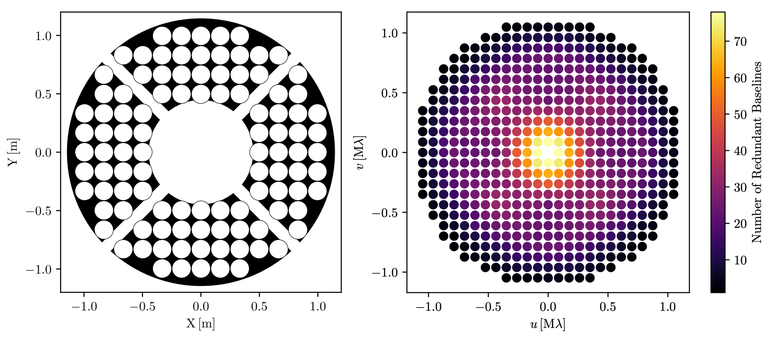

Figure 1: *Left*: HST aperture (black) and simulated sub-apertures (white circles). *Right*: The corresponding baselines (at 1.7 μm), colored by their redundancy. The 104 simulated sub-apertures sample 258 unique baselines and generate 206 kernel-phases.

Each pair of apertures, or baseline, contributes both the true phase of the source and a phase error from each of the apertures. Combining all the baselines, we can write a matrix equation for the measured phases:

$$\mathbf{\Phi} = \mathbf{\Phi}_\circ + \mathbf{A} \cdot \phi \qquad (1)$$

Where Φ a vector of the measured phases from each baseline, Φ_0 is the true source phase, **A** is a matrix encoding which apertures contribute to each baseline, and ϕ is the phase errors of each aperture. Columns and rows of **A** correspond to apertures and baselines, respectively.

To remove the phase errors, we calculate the kernel (**K**) of **A**:

$$\mathbf{K} \cdot \mathbf{A} = 0 \qquad (2)$$

We can then multiply both sides of Equation 1 by **K** to get

$$\mathbf{K} \cdot \mathbf{\Phi} = \mathbf{K} \cdot \mathbf{\Phi}_\circ + \mathbf{K} \cdot \mathbf{A} \cdot \phi = \mathbf{K} \cdot \mathbf{\Phi}_\circ \qquad (3)$$

This produces observables called kernel-phases (first presented by Martinache 2010) which are independent of phase errors, similar to closure-phases used with NRM. **This technique can achieve similar detection limits to NRM in a fraction of the time and can be applied to dimmer sources where NRM is not feasible, as well as to archival data sets.**

From Image to Kernel-Phase to Detections & Limits

We have analyzed the entire NICMOS1 archive of observations of brown dwarfs (in F110W and F170M) to search for compact binary systems. **We fit the data using a Bayesian routine** (`PyMultiNest`; Buchner et al. 2014) **and calculate detection limits using a similar method to NRM**. New realizations of the noise are created by scrambling the model subtracted kernel-phases. We then fit the contrast on a grid in separation and PA and the 99% confidence contrast is the contrast at which 99% of all fits are fainter. Fig. 2 & 3 show the analysis and results of our survey. Our pipeline is open source and available at: **https://github.com/smfactor/argus**

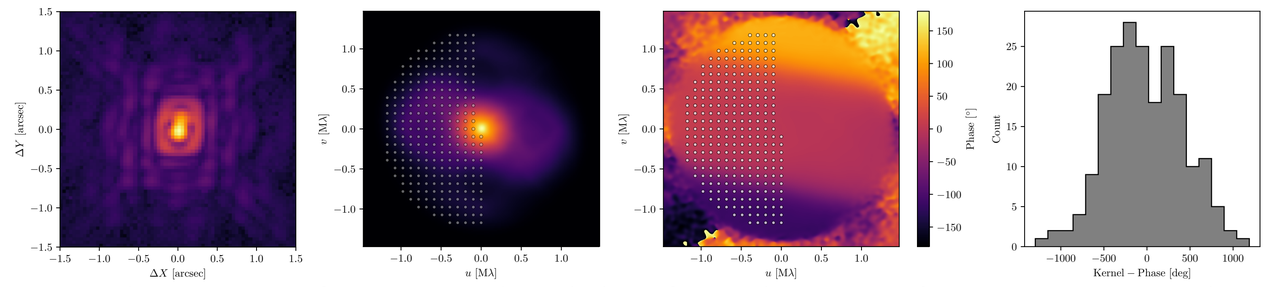

Figure 2: The progression from image to kernel-phase for an observation of 2MASS J0147-4954, a brown dwarf with a companion at ~140 mas (~1 λ/D) and ~2:1 contrast in F170M. F*rom left to right*: NICMOS1 image (fourth root scaling), Fourier-amplitude, Fourier-phase (grey circles show the model baselines from Fig. 1), and resulting kernel-phases. Science target kernel-phases must then be calibrated by subtracting the kernel-phases from a singular source.

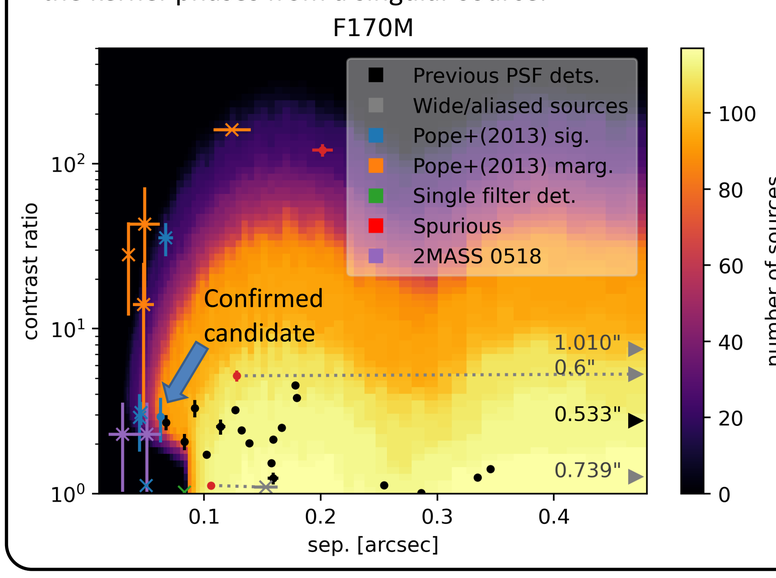

Figure 3: Stacked 5σ detection limits for the survey. Filled circles indicate detected companions while X's indicate non-detections (literature values). Colors correspond to initial detection methods. **We confirm one (2MASS 2351-2537, blue circle with arrow) of the significant candidates from Pope et al. (2013)** but none of the other candidates. Spurious detections (connected to the literature values) are a triple system, low SNR observation, and a bad pixel. Images of 2MASS 0518-2828 show an elongated PSF in F090M (not analyzed) but we do not detect a companion in F110W or F170M.

Results: A BD population strongly favoring tightly bound equal mass companions

We fit our detections with a companion frequency F, mass ratio (q) power-law index γ, and log-normal projected separation mean $\overline{\log(\rho)}$ and $\sigma_{\log(\rho)}$. Flux ratios were converted to mass ratios using Filippazzo et al. (2015) bolometric corrections and ATMO2020 models (Phillips et al. 2020) assuming a range of field ages. The unresolved ($\rho < 1$ au) companion frequency was limited to $2.5^{+8.6}_{-2.6}$% (Blake et al. 2010). **We find a companion distribution centered at a tighter separation than previous studies** (due to our higher angular resolution) **that strongly favors equal mass companions** ($q \sim 1$). Fig. 4 shows these distributions and Fig. 5 puts them in context.

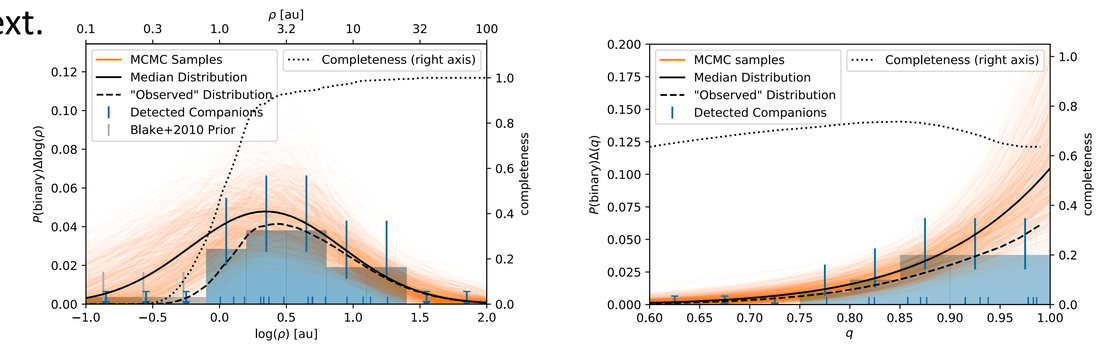

Figure 4: Binary population vs. projected separation (*left*) and mass ratio (*right*). The blue histogram and ticks show detected companions. The MCMC samples (orange) and median distribution (solid black) use the following parameters: $\boldsymbol{F = 0.22^{+0.07}_{-0.06}}$, $\boldsymbol{\overline{log(\rho)} = 0.35^{+0.19}_{-0.25}}$ **or** $\boldsymbol{\overline{\rho} = 2.2^{+1.2}_{-1.0}}$ **au,** $\boldsymbol{\sigma_{\log(\rho)} = 0.58^{+0.20}_{-0.13}}$**, and** $\boldsymbol{\gamma = 9^{+3}_{-2}}$ (using an assumed field age of 1.9 Gyr).

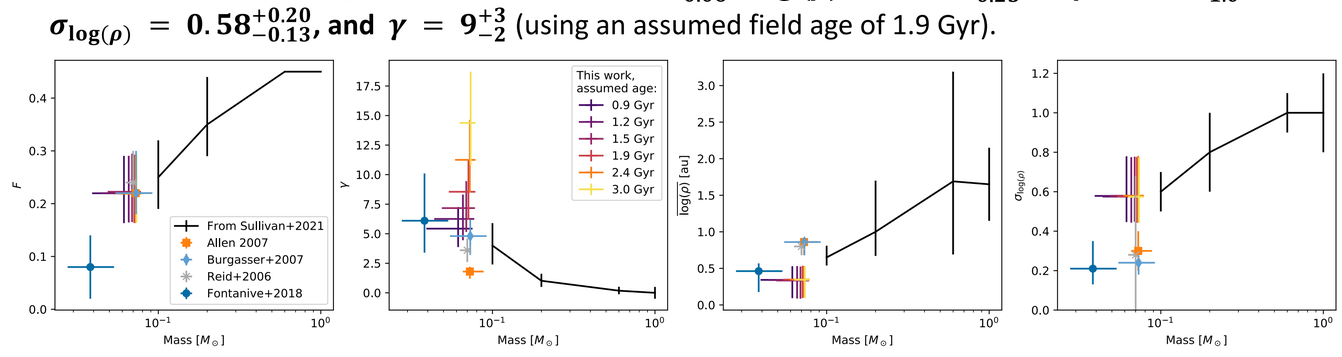

Figure 5: Binary demographics as a function of primary mass, comparing the results from this work to previous studies. Literature sources are given in the legend. Results from this work are shown on a color scale for different assumed field ages, which only affects the derived masses and therefore γ.